

Metal for Plasmonic Ultraviolet Laser: Al or Ag?

Yu-Hsun Chou, Kuo-Bin Hong, Yi-Cheng Chung, Chun-Tse Chang, Bo-Tsun Chou, Tzy-Rong Lin, *Member, IEEE*, Sergei M. Arakelian, Alexander P. Alodjants, and Tien-Chang Lu, *Senior Member, IEEE*

Abstract—Surface plasmon polariton (SPP) nanolasers have recently emerged as promising candidates for generating a coherent light source in nanophotonic integration circuits. The properties of SPP nanolasers, such as group velocity, mode area, modulation speed, and threshold performance, can be manipulated using a dispersion relation. In this study, we investigated the characteristics of SPP nanolasers operated near and far from the SP frequency. Our results indicated that SPP nanolaser performance can be significantly influenced by manipulating the dispersion relation.

Index Terms—Aluminum, nanowire, plasmonic laser, silver, surface plasmon, zinc oxide (ZnO).

I. INTRODUCTION

THE use of small optoelectronic devices with low power consumption for realizing high-density integrated optoelectronic circuits has attracted increasing attention in recent years [1]–[3]. Although current semiconductor device manufacturing technology enables the development of nanoscale semiconductor optoelectronics, such devices are restricted by the optical diffraction limit and cannot be downscaled further. Recently, a new type of nanoscale cavity has emerged that involves the localization of plasmons at the metal–insulator interface. These localized modes at the interface are referred to as surface plasmon polaritons (SPPs) [4]. The use of diffraction-unlimited plasmons has been successfully demonstrated in applications such as super-resolution optical microscopy, photolithography, photovoltaics, chemical sensing, and nanolasers [5]–[9]. An extremely small volume of field occupation at the microscale occupation at the microscale and nano-scale for potentially scalable photonic devices provides a new avenue in modern quantum information technologies [10]–[12].

Manuscript received January 31, 2017; revised May 1, 2017 and June 26, 2017; accepted August 30, 2017. Date of publication September 4, 2017; date of current version September 14, 2017. This work was supported in part by the Ministry of Education Aim for the Top University Program, in part by the Minister of Science and Technology (MOST) under Contracts 104-2923-E-009-003-MY3 and 103-2221-E-019-028-MY3, and in part by the Russian Foundation for Basic Research, Russia under Grants 15-59-30406 and 15-52-52001. (*Corresponding author: Tien-Chang Lu.*)

Y.-H. Chou, K.-B. Hong, C.-T. Chang, B.-T. Chou, and T.-C. Lu are with the National Chiao Tung University, Hsinchu 300, Taiwan (e-mail: timothychou.cop99g@hotmail.com; kbhong@mail.nctu.edu.tw; pigcat0938@gmail.com; choubotsun@gmail.com; timtclu@mail.nctu.edu.tw).

Y.-C. Chung and T.-R. Lin are with the National Taiwan Ocean University, Keelung 202, Taiwan (e-mail: whitesheep29@gmail.com; trlin@ntou.edu.tw).

S. M. Arakelian is with the Stoletov's Vladimir State University, Vladimir 600000, Russia (e-mail: arak@vlsu.ru).

A. P. Alodjants is with the VSU and ITMO University, Saint Petersburg 197101, Russia (e-mail: alexander_AP@list.ru).

Color versions of one or more of the figures in this paper are available online at <http://ieeexplore.ieee.org>.

Digital Object Identifier 10.1109/JSTQE.2017.2748521

Recently, semiconductor–insulator–metal (SIM) waveguides have become one of the most frequently employed plasmonic structures that confine the electromagnetic field beyond the optical diffraction limit. Currently, SIM structures are widely used in nanolasers at different wavelengths from the ultraviolet (UV) to visible regions [13]–[18]. By carefully selecting a material combination with appropriate insulator thickness, the distribution of the electromagnetic field in SIM structures can be compressed to a subwavelength scale. An extremely small mode distribution enhances the interaction between light and matter by increasing the Purcell factor, which is beneficial for laser operations in a nanoscale cavity [13]–[16]. Similar to any microcavity, these confined modes can interact with other excitations such as excitons in semiconductors. Therefore, energy can be amplified in nanoscale cavities in a manner similar to that in traditional microcavities. Several studies have conducted laser operations in SIM structures, with a gain medium placed on a metal film and separated by a thin dielectric layer to compensate for ohmic losses [8], [13]–[16], [19], [20]. The most widely used gain media for SIM structures are semiconductor nanowires (NWs), which can naturally form a Fabry–Perot-type SP cavity.

Recently, nanolaser development through SPP manipulations has attracted increased attention in the construction of ultra-compact integrated optoelectronic devices and systems [21]–[23]. The characteristics of SPPs can be determined by the dispersion relation of devices, which is influenced by the material's permittivity and structural parameters [24]–[28]. An alternative method for manipulating the dispersion relation of SPP nanolasers relies on the thickness control of the insulation layer between a semiconductor and a metal thin film [29]. However, the manipulation range of the dispersion relation is limited by material characteristics. To investigate the characteristics of SPP nanolasers with substantial dispersion differences, we selected SPP nanolasers with silver- and aluminum-based thin films to analyze the differences between SPP lasers operating near and those operating far from the SP frequency. Because Ag has an interband transition at 350 nm, the dispersion relation of SPs near 370 nm is bent [18]. To understand the characteristics of SPP nanolasers operating near and far from the SP frequency, we selected a semiconductor with a bandgap near 370 nm as the gain medium. Aluminum and silver are not only useful for visible and UV optoelectronic applications but also provide an excellent test bed for exploring quantum plasmonic effects [30], such as ultrafast modulation [17], strong interactions between excitons and SPs [18], and high characteristic temperatures [31]. For highly reliable SPP laser operation, ZnO NWs provide

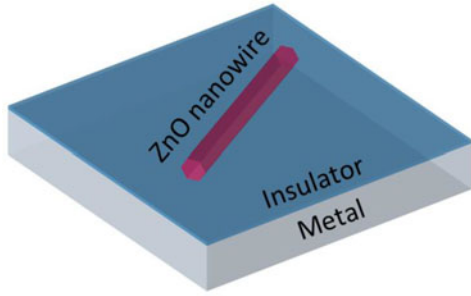


Fig. 1. ZnO SPP nanolaser with a SIM structure.

exciton binding energies greater than the thermal energy at room temperature (25.6 meV) and strong oscillation strength for interacting with SPPs [32]. Therefore, ZnO NWs are the most suitable material for stable SPP laser operation under different operating conditions.

II. DEVICE STRUCTURE AND SIMULATION

In this study, we evaluated SIM structures with ZnO NWs placed on different metal substrates (see Fig. 1). Therefore, SPs can be localized at the metal–dielectric layer interface. The oscillation electrons in metals can couple with the excitation electromagnetic wave and form SPPs. For SPPs with large wave vectors, the operation frequency approaches the characteristic SP frequency [33]:

$$\omega_{sp} = \frac{\omega_p}{\sqrt{1 + \epsilon_d}} \quad (1)$$

where ω_p is the plasmon frequency of the metal and ϵ_d is the dielectric constant of the material contact to the metal surface. According to (1), the SP frequency for Al ($\omega_{sp}^{Al} = 1.4 \times 10^{15}$ Hz) is far from the ZnO bandgap energy frequency, whereas that for Ag ($\omega_{sp}^{Ag} = 8.3 \times 10^{14}$ Hz) is near the ZnO bandgap energy frequency ($\omega_{ex}^{ZnO} = 8.6 \times 10^{14}$ Hz). To illustrate the differences between SPP nanolasers operated far from and those operated near the SP frequency, the fundamental dispersion relations of ZnO NWs (side length, $d = 35$ nm) placed on SiO₂ (thickness, $h = 7$ nm) with different metal substrates (Al or Ag) are shown in Fig. 2(a) and (b), and the corresponding group indices calculated as $n_g = c_0 d\omega/d\beta$ were 5.7 and 79, respectively, where c_0 is the speed of light in vacuum. To investigate the field distribution, we used the finite element method [34]. For devices with Al substrates, the SP frequency was at least 1.5 times higher than the ZnO bandgap energy frequency; therefore, the electric field partially dissipated into the air [see Fig. 2(c)]. By contrast, Ag had a strong material dispersion relation in the UV region; therefore, the SP frequency was near the ZnO bandgap energy frequency. Furthermore, strong plasmonic effects reduced the mode profile into extremely small regions compared with those in Al samples [see Fig. 2(d)]. The SPs were confined at a wavelength of 370 nm with an effective mode area of $4.8 \times 10^{-3} \lambda^2$ for Al and $1.3 \times 10^{-3} \lambda^2$ for Ag.

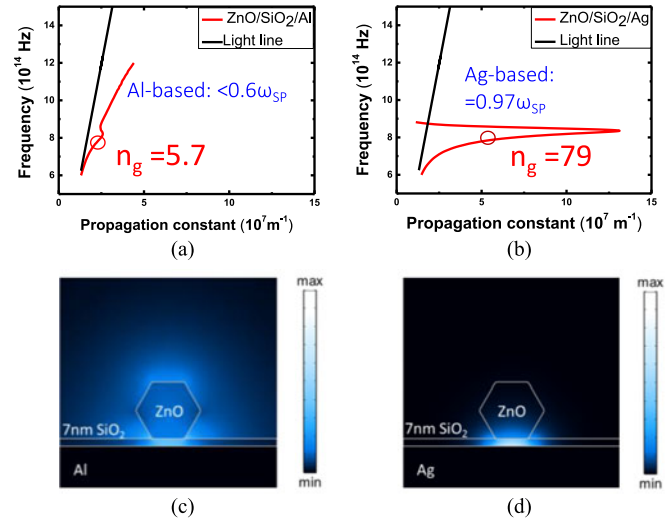


Fig. 2. Dispersion curve of fundamental SPP modes of (a) Al-based nanolaser. (b) Ag-based nanolaser. (c) and (d) show the electric field distributions of fundamental SPP modes inside nanolasers.

III. EXPERIMENTAL RESULTS

A. Device Fabrication and Measurement Setup

We used GaAs (100) substrates for depositing Al thin films. After the substrate was treated with rapid thermal annealing, a 200-nm-thick aluminum film was deposited through molecular beam epitaxy onto the substrate [35]. For the Ag-based ZnO SPP laser, we used an electron-gun evaporation system to deposit a 200-nm-thick Ag film on a silicon (100) wafer. After the metal film was deposited, a 7-nm-thick SiO₂ film was deposited using an electron-gun evaporator. To identify the precise locations of individual NWs on the metal film, we used a gold pattern on the SiO₂ insulation layer. Single-crystalline ZnO NWs with an average side length (d) of 35 nm were fabricated using the hydrothermal method [36] and placed onto the patterned substrate after insulator deposition. To compare the optical performance of ZnO NWs on Al- and Ag-based substrates, both samples were placed into a cryogenic chamber with a controlled ambient temperature. The fabricated device was mounted in a cryostat chamber, and the excitation beam was split by a 50:50 dichroic mirror to monitor the power of the incident beam. The beam generated by a Nd:YVO₄ 355-nm pulse laser, with a 0.5-ns pulse width and 1-kHz repetition rate, was launched into a 100 \times near-UV high-magnification objective lens (numerical aperture = 0.55) with a focal spot size diameter (D) of 15 μ m to focus on a single NW. To measure the polarization of emission signals, a polarizer was placed in front of the fiber. Photons emitted from the ZnO SPP nanolaser were collected by the same objective lens and transmitted through a UV optical fiber into a monochromator with a spectral resolution of 0.2 nm (see Fig. 3). Because the coordinates of a single NW were already verified through scanning electron microscopy, we used a white lamp to illuminate the device surface and capture the location of the single NW using a CCD camera on the monitor. To confirm that the signals detected by the spectrometer originated from a single ZnO NW,

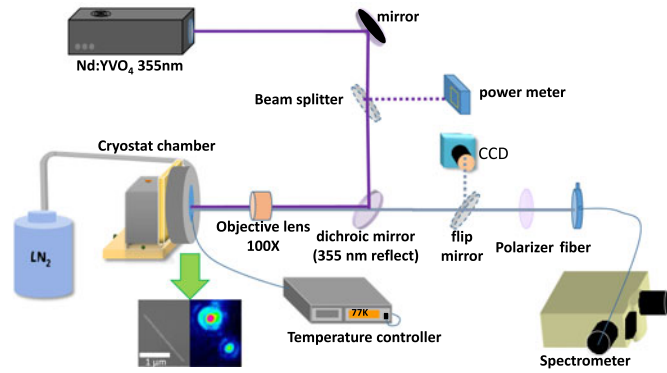


Fig. 3. Micro photoluminescence spectroscopy. Samples were mounted into a temperature-controlled vacuum chamber and optically pumped by the third harmonic generation of a Nd:YVO₄ 355-nm pulse laser at different ambient temperatures. Incident beams were focused by a 100× near-UV infinity-corrected objective lens with a numerical aperture of 0.55. Inset shows the emission profile of the ZnO NW.

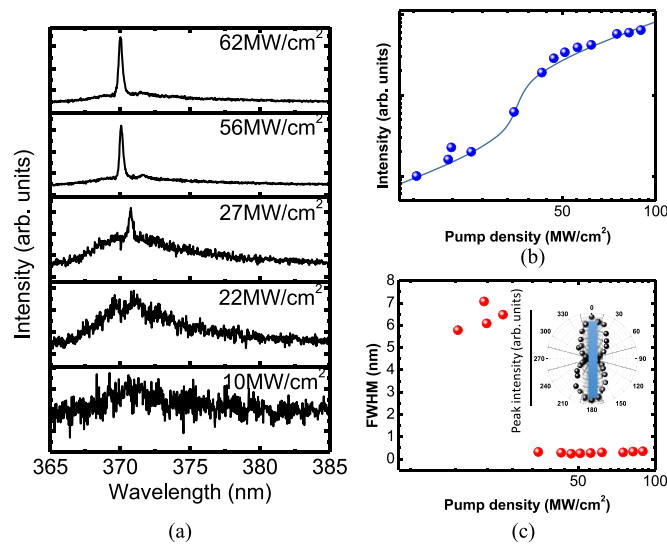


Fig. 4. (a) Measured spectra at a laser pumping power density of 10–62 MW/cm². (b) L–L curve of the emission peak at 370 nm. The solid lines represent the fitted results calculated using simplified rate equations. The extracted spontaneous coupling factor (β) is 0.1. (c) Linewidth of the emission peak versus pumping power density. Inset shows the corresponding polar plot of emission intensity. The polarization direction of the lasing mode is parallel to the NW.

a laser profiler was used to record the emission profiles of the NW (inset, Fig. 3).

B. Optical Properties of the Devices

Fig. 4(a) shows the spectra and lasing characteristics of ZnO NWs placed on Al with a 7-nm SiO₂ insulation layer at 77 K. Lasing emission was observed with a linewidth narrowed from 6 to 0.4 nm. A nonlinear behavior of the light-in-light-out (L–L) curve with a pumping threshold (P_{th}) of 27 MW/cm² was clearly observed in the Al sample. The lasing mode was highly polarized in the direction parallel to the NW [inset, Fig. 4(c)]. The direction of polarization indicated that the observed modes

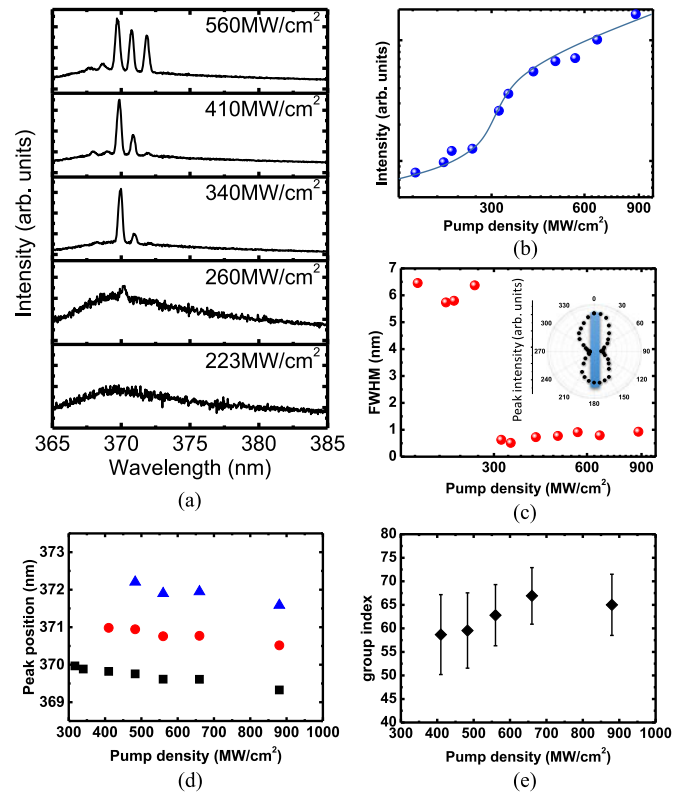


Fig. 5. (a) Measured spectra of the Ag sample at a laser pumping power density of 223–560 MW/cm². (b) L–L curve of the emission peak at 370 nm. The solid lines represent the fitted results calculated using simplified rate equations. The extracted spontaneous coupling factor (β) is 0.2. (c) Linewidth of the emission peak versus pumping power density. Inset shows the corresponding polar plot of emission intensity. The polarization direction of the lasing modes is parallel to the NW. (d) Peak positions extracted from the emission spectra. (e) Calculated group index above the threshold.

belonged to the fundamental SP mode. Due to smooth changes of the dispersion gradient, single-mode operation was achieved by selecting material combinations (ZnO/SiO₂/Al) with an SP frequency far from the operation frequency ($<0.6 \omega_{SP}$).

For samples having an operation frequency ($0.97 \omega_{SP}$) near the SP frequency, multiple longitudinal modes were observed under a higher pumping density [see Fig. 5(a)]. The broad PL linewidth narrowed to 0.5 nm at a pumping threshold (P_{th}) of 260 MW/cm². The observed mode spacing was approximately 1 nm [see Fig. 5(d)], and the corresponding group index, 65, can be calculated as $\Delta\lambda = \lambda^2 / (2n_g L)$ [see Fig. 5(e)]. Such large group indices are mainly caused by drastic changes in the dispersion relation near the operation frequency. The polarization direction of all peaks [see Fig. 5(a)] was parallel to the ZnO NW direction, which is consistent with the fundamental SP mode. Therefore, when a material combination (ZnO/SiO₂/Ag) with an SP frequency near the operation frequency ($0.97 \omega_{SP}$) is selected, the highly dispersive SP mode leads to an extremely large group index with mode confinement in an ultra-small region.

To further understand the differences between SPP nanolasers operated far from and near the SP frequency, we calculated the transparency gain as $g_{tr} = 1 / (L_p \cdot \Gamma_{wg})$, which is defined as the gain for which energy can travel through the SIM waveguide

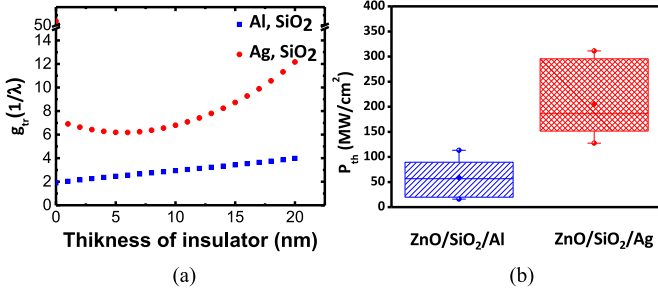


Fig. 6. (a) Calculated normalized transparency threshold gain of the fundamental SPP mode in ZnO NWs placed on Al/SiO₂ and Ag/SiO₂ films. (b) Average threshold quarter box chart of 13 NWs on different metal substrates with a 7-nm SiO₂ insulation layer.

without dissipation. The propagation length (L_p) was defined as the distance at which energy falls to $1/e$ and was determined using the imaginary part of the mode propagation constant k_z as $L_p = 1/[2\text{Im}(k_z)]$; Γ_{wg} is the waveguide confinement factor of the SIM structure, which indicates the overlapping of the portion of a mode with the gain medium and is defined as the ratio of the modal gain to the material gain in the active region. This factor can be expressed as previously described in [37] as follows: $\Gamma_{wg} = (n_a/2\eta_0) \int_{A_a} |E(\rho)|^2 d\rho/P_z$, where $E(\rho)$ is the electric field expressed in cylindrical coordinates; P_z is the power flow in the propagation direction; n_a is the refractive index of the gain medium; A_a is the region of the gain medium; and η_0 is the intrinsic impedance. Fig. 6(a) shows the transparency gain normalized to the operation wavelength. Although the Ag-based SPP nanolaser benefitted from the dispersive SP mode with a large waveguide confinement, it had a shorter propagation length. The trade-off between the confinement factor and propagation length resulted in an extreme minimum of transparency gain at $h_{\text{SiO}_2} = 7$ nm [18]. Compared with the Ag-based SPP nanolaser, the Al-based SPP nanolaser ($<0.6 \omega_{\text{SP}}$) offered a favorable trade-off between the mode confinement and propagation length. Moreover, when the appropriate material combination was selected on the basis of the material's permittivity, the minimum transparency gain was achieved at an insulator thickness of zero [31]. To verify the transparency gain of SPP nanolasers with different SP dispersion relations, the threshold performance was compared between the Al- and Ag-based SPP nanolasers. The Ag-based SPP nanolaser had an average threshold density of approximately 190 MW/cm², which is three times higher than that of the Al-based SPP nanolaser [see Fig. 6(b)]. The simulation and experimental results revealed that the SPP nanolaser operated near the SP frequency had a higher transparency threshold gain than that operated far from the SP frequency. Both the simulation and experimental results reveals that for SPP nanolaser operating nearby the SP frequency has a higher transparency threshold gain than the SPP nanolaser operating away from the SP frequency.

C. Temperature Characteristic and Rate Equation

We compared the evolution of SPP energy with other ZnO excitations across a wide temperature range [38]–[42]. The lasing peak energies of the Al- and Ag-based ZnO SPP nanolasers

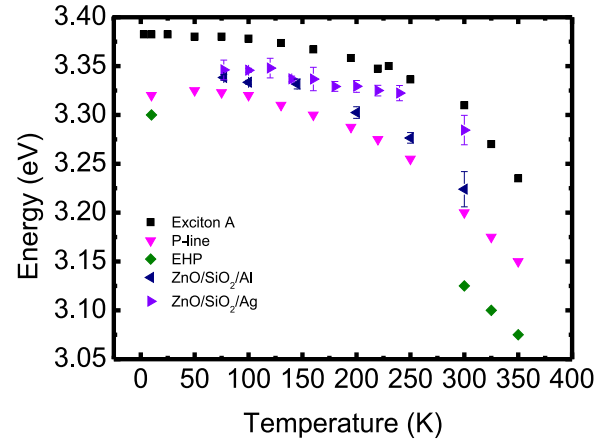


Fig. 7. Temperature-dependent excitation peaks in ZnO and fabricated ZnO SPP nanolasers.

were far from the electron-hole plasma (EHP) peaks between 77 K and room temperature (see Fig. 7). The lasing peak energies of the Al- and Ag-based ZnO SPP nanolasers were between the exciton absorption peak (Exciton A) and the P -line (exciton–exciton collision) emission peaks. This finding confirmed that the optical gain from the ZnO SPP nanolasers did not originate from EHP, which requires the carrier density to be higher than the exciton Mott density (for ZnO at 300 K, $n_{\text{mott}} = 0.5 \times 10^{17} \text{ cm}^{-3} \sim 4 \times 10^{17} \text{ cm}^{-3}$ [41], [42]).

The energy split from the exciton mode was approximately 60 meV for both samples at 77 K, probably due to exciton–SP coupling. In addition, the energy split decreased slightly toward the heating process because of the decreased Purcell factor and lower coupling rate. To further understand the evolution of exciton and SP densities in SPP nanolasers, the following two coupling rate equations for n (exciton density) and s (SP density) with various contribution and dissipation terms were employed [18]:

$$\frac{dn}{dt} = \eta\eta'P - An - g_0(n - n_{\text{tr}})s \quad (2)$$

$$\frac{ds}{dt} = \Gamma_{wg}\beta An + \Gamma_{wg}g_0(n - n_{\text{tr}})s - \gamma s \quad (3)$$

For simplification, only one SP mode was considered, and the exciton distribution in the NW after excitation was treated uniformly. The injection efficiency of the ZnO NW was assumed to be $\eta = 0.1 \text{ cm}^{-1}$. The pumping ratio was estimated as $\eta' = S_{\text{NW}}/S_{\text{spot}}$, where the scattering cross section of a NW was defined as $S_{\text{NW}} = Ld(\pi d/\lambda)^2$, and the excitation area of the laser spot was defined as $\pi D^2/4$. P is the excitation power density; β is the spontaneous emission factor; A is the average spontaneous emission rate of the ZnO exciton with $A = F/\tau_r$, where τ_r is the spontaneous emission lifetime of the ZnO NW, which was 248 ps from the measured value, and F is the effective Purcell factor, which was 15 for the Al sample and 67 for the Ag sample; g_0 is the differential gain of ZnO and is proportional to the Purcell factor and group velocity $v_g = c/n_g$, where c is the speed of light and n_g denotes the calculated group index of the SP mode; $n_{\text{tr}} = 1 \times 10^{17} \text{ cm}^{-3}$ is the transparent exciton

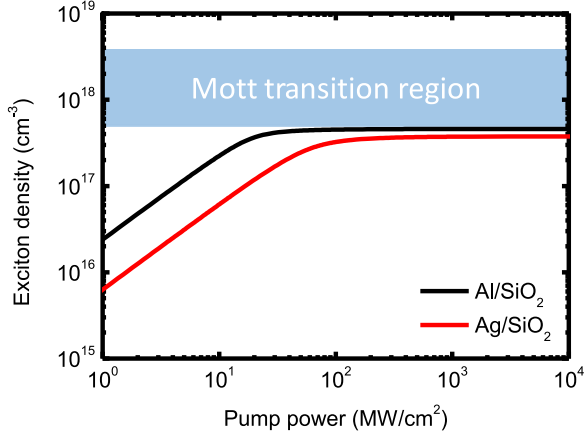


Fig. 8. Exciton density as a function of pumping power for ZnO SPP nanolasers on the Al/SiO₂ and Ag/SiO₂ of the ZnO surface plasmon nanolaser with SIM structure. The light blue region shows the lower bound [41] and upper bound [42] of ZnO Mott density (bulk@300 K).

density [32]; and γ refers to the SPP loss rate [18]. The exciton and SPP densities in a steady-state regime are represented by (2) and (3), with $dn/dt = 0$ and $ds/dt = 0$. In the steady state, the SP density is given by

$$s = \frac{\Gamma\beta An}{\gamma - \Gamma g_0(n - n_{tr})} \quad (4)$$

According to (4), threshold conditions can be achieved when the denominator approaches zero, and the guided lines of L-L curves with fitted β factors for different nanolaser structures can be obtained by using steady-state equations. The mode inside the nanolaser was tightly confined, resulting in a confinement factor Γ larger than unity and a Purcell factor F that was two orders of magnitude larger than that of conventional lasers. In this study, the large Purcell factor and strong confinement factor suppressed the exciton density to exceed the Mott transition region under the threshold condition [32], [41], [42].

Fig. 8 shows the evolution of exciton density with an increase in the pumping density for NWs lying on Ag and Al films with a 7-nm-thick SiO₂ insulation layer. The exciton density above the threshold of samples with SiO₂/Ag and SiO₂/Al structures remained below the ZnO bulk exciton Mott density (300 K), ensuring efficient coupling between excitons and SPs. In addition, it has been reported that system with reduced dimensionality will have more stabilized exciton properties, and the Mott density in ZnO NW might be higher than the ZnO bulk [43].

The turn-on behaviors of the Ag or Al based SPP nanolasers in Fig. 9 are calculated based on the simple rate equations shown above. As shown in Fig. 9, relaxation frequencies up to 10 THz and 4 THz can be observed for Ag and Al based SPP nanolasers above the threshold. Such a fast relaxation process is due to the large Purcell factor that drastically reduces the carrier recombination lifetime and the extremely small cavity with a short plasmon lifetime. It should be noted that our simulation did not take into account the gain saturation effect, relaxation and diffusion times of exciton, which would impede such a high relaxation frequency. More elaborate analyzed on direct modulation speed of nanolaser were discussed by K. Ding *et al.* [44].

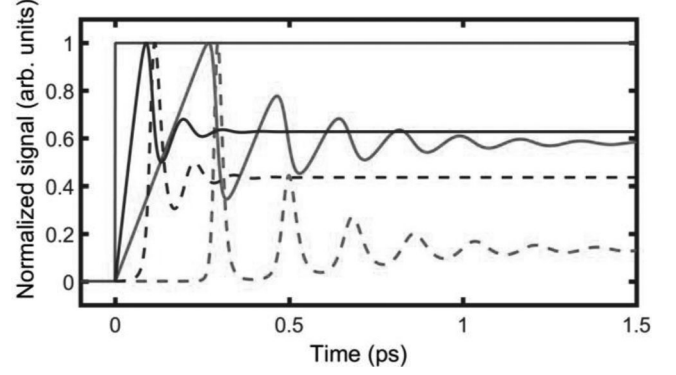


Fig. 9. Turn-on dynamics of Ag/SiO₂/ZnO SPP nanolasers (blue) and Al/SiO₂/ZnO SPP nanolasers (red). The brown line is the normalized pumping signal. The solid and dashed lines represent exciton and SP densities, respectively, as functions of time.

Here, our preliminary demonstration of such high relaxation frequency realized in a nanoscale light emitters shall be very promising in the future high speed and high density information applications.

IV. CONCLUSION

Our work reveals the importance of dispersion relation control in plasmonic devices and paves the way for application of ultraviolet nanolasers in areas such as optical communications, data storage, subwavelength imaging, and biosensing. In this study, both the Al- and Ag-based SPP nanolasers sustained up to room temperature with high-quality films. In addition, single-mode operation was achieved by selecting metal combinations with an SP frequency far from the operation frequency. For metals with an SP frequency near the operation frequency, multiple longitudinal modes were observed. The theoretical group indices calculated using $n_g = c_0(d\omega/d\beta)$ were 5.7 and 79, respectively. For the Ag-based SPP nanolaser operating near the SP frequency, multiple longitudinal modes with large group indices and ultra-compact mode areas were supported by a strong dispersion relation near the operation frequency. By contrast, the Al-based SPP nanolaser operating far from the SP frequency had small group indices with larger mode areas and could support only single-mode operation for ZnO NWs with a length (L) of 1–2 μm . By balancing the trade-off between the waveguide confinement factor and propagation length, the threshold of the Al-based SPP nanolaser was much lower than that of the Ag-based SPP nanolaser. Our results indicate that the characteristics of SPP nanolasers can be manipulated by selecting metals with different SP frequencies. Moreover, the ultra-compact mode areas and strong interactions between SPs and excitons provide a new class of coherent sources for quantum plasmonic test beds.

ACKNOWLEDGMENT

The authors would like to thank Prof. S.-C. Wang, Prof. H.-C. Kuo, Prof. S.-D. Lin, T.-C. Chang, and P.-J. Cheng from the National Chiao Tung University, Hsinchu, Taiwan.

REFERENCES

- [1] A. V. Krishnamoorthy *et al.*, "Computer systems based on silicon photonic interconnects," *Proc. IEEE*, vol. 97, pp. 1337–1361, Jul. 2009.
- [2] X. Chen *et al.*, "Device engineering for silicon photonics," *NPG Asia Mater.*, vol. 3, pp. 34–40, Jan. 2011.
- [3] Z. Zhou *et al.*, "On-chip light sources for silicon photonics," *Light Sci. Appl.*, vol. 4, Nov. 2015, Art. no. e358.
- [4] S. L. Chuang, *Physics of Photonic Device*. New York, NY, USA: Wiley, 2008.
- [5] F. Wei *et al.*, "Wide field super-resolution surface imaging through plasmonic structured illumination microscopy," *Nano Lett.*, vol. 14, pp. 4634–4639, Jul. 2014.
- [6] X. Luo *et al.*, "Subwavelength photolithography based on surface-plasmon polariton resonance," *Opt. Express*, vol. 12, pp. 3055–3065, Jul. 2004.
- [7] H. A. Atwater *et al.*, "Plasmonics for improved photovoltaic devices," *Nature Mater.*, vol. 9, pp. 205–213, Feb. 2010.
- [8] R. M. Ma *et al.*, "Explosives detection in a lasing plasmon nanocavity," *Nature Nanotechnol.*, vol. 9, pp. 600–604, Jul. 2014.
- [9] S. Noda, "Seeking the ultimate nanolaser," *Science*, vol. 314, no. 5797, pp. 260–261, Oct. 2006.
- [10] A. V. Akimov *et al.*, "Generation of single optical plasmons in metallic nanowires coupled to quantum dots," *Nature*, vol. 450, pp. 402–406, Nov. 2007.
- [11] R. W. Heeres *et al.*, "Quantum interference in plasmonic circuits," *Nature Nanotech.*, vol. 8, pp. 719–722, Aug. 2013.
- [12] E. S. Sedov *et al.*, "Tunneling-assisted optical information storage with lattice polariton solitons in cavity-QED arrays," *Phys. Rev. A*, vol. 89, 2014, Art. no. 033828.
- [13] R. F. Oulton *et al.*, "Plasmon lasers at deep subwavelength scale," *Nature*, vol. 461, pp. 629–632, 2009.
- [14] R.-M. Ma, R. F. Oulton, V. J. Sorger, G. Bartal, and X. Zhang, "Room temperature sub-diffraction-limited plasmon laser by total internal reflection," *Nature Mater.*, vol. 10, pp. 110–113, 2011.
- [15] Y.-J. Lu *et al.*, "Plasmonic nanolaser using epitaxially grown silver film," *Science*, vol. 337, pp. 450–453, 2012.
- [16] Q. Zhang *et al.*, "A room temperature low-threshold ultraviolet plasmonic nanolaser," *Nature Commun.*, vol. 5, Sep. 2014, Art. no. 4953.
- [17] T. P. Sidiropoulos *et al.*, "Ultrafast plasmonic nanowire lasers near the surface plasmon frequency," *Nature Phys.*, vol. 10, pp. 870–876, 2014.
- [18] Y.-H. Chou *et al.*, "Ultrastrong mode confinement in ZnO surface plasmon nanolasers," *ACS Nano*, vol. 9, pp. 3978–3983, Apr. 2015.
- [19] M. T. Hill *et al.*, "Lasing in metal-insulator-metal sub-wavelength plasmonic waveguides," *Opt. Express*, vol. 17, pp. 11107–11112, 2009.
- [20] M. Noginov *et al.*, "Demonstration of a spaser-based nanolaser," *Nature*, vol. 460, pp. 1110–1112, Aug. 2009.
- [21] C. Ropers *et al.*, "Grating-coupling of surface plasmons onto metallic tips: A nanoconfined light source," *Nano Lett.*, vol. 7, pp. 2784–2788, Sep. 2007.
- [22] V. J. Sorger, R. F. Oulton, R. M. Ma, and X. Zhang, "Toward integrated plasmonic circuits," *MRS Bull.*, vol. 37, pp. 728–738, Aug. 2012.
- [23] G. Lerosey, D. F. P. Pile, P. Mathieu, G. Bartal, and X. Zhang, "Controlling the phase and amplitude of plasmon sources at a subwavelength scale," *Nano Lett.*, vol. 9, pp. 327–331, Jan. 2009.
- [24] J. Wang, Q. Fan, H. Zhang, and T. Xu, "Research progress in plasmonic structural colors," *Opto-Elect. Eng.*, vol. 44, pp. 22–33, Jan. 2017.
- [25] E. Lier, D. H. Werner, C. P. Scarborough, Q. Wu, and J. A. Bossard, "An octave-bandwidth negligible-loss radiofrequency metamaterial," *Nature Mater.*, vol. 10, pp. 216–222, Jan. 2011.
- [26] Y. Guo *et al.*, "Dispersion management of anisotropic metamirror for super-octave bandwidth polarization conversion," *Sci. Rep.*, vol. 5, Jan. 2015, Art. no. 8434.
- [27] D. Ye *et al.*, "Ultrawideband dispersion control of a metamaterial surface for perfectly-matched-layer-like absorption," *Phys. Rev. Lett.*, vol. 111, Oct. 2013, Art. no. 187402.
- [28] M. Pu *et al.*, "Spatially and spectrally engineered spin-orbit interaction for achromatic virtual shaping," *Sci. Rep.*, vol. 5, May 2015, Art. no. 9822.
- [29] B. T. Chou *et al.*, "Realization of UV plasmonic nanolasers with extremely small mode volume," *IEEE J. Sel. Topics Quantum Electron.*, vol. 21, no. 6, Nov./Dec. 2015, Art. no. 1503106.
- [30] D. Ge' rard and S. K. Gray, "Aluminium plasmonics," *J. Phys. D Appl. Phys.*, vol. 48, 2015, Art. no. 184001.
- [31] Y. H. Chou *et al.*, "High-operation-temperature plasmonic nanolasers on single-crystalline aluminum," *Nano Lett.*, vol. 16, pp. 3179–3186, Apr. 2016.
- [32] U. Ozgur *et al.*, "A comprehensive review of ZnO materials and devices," *J. Appl. Phys.*, vol. 98, 2005, Art. no. 041301.
- [33] S. A. Maier, *Plasmonics: Fundamentals and Applications*. New York, NY, USA: Springer, 2007.
- [34] COMSOL Inc., "Comsol multiphysics OULTs," COMSOL Inc., Burlington, MA, USA, 2014.
- [35] H. W. Liu *et al.*, "Single-crystalline aluminum nanostructures on a semi-conducting GaAs substrate for ultraviolet to near-infrared plasmonics," *ACS Nano*, vol. 9, no. 4, pp. 3875–3886, Apr. 2015.
- [36] B. Liu and H. C. Zeng, "Hydrothermal Synthesis of ZnO nanorods in the diameter regime of 50 nm," *J. Amer. Chem. Soc.*, vol. 125, pp. 4430–4431, Mar. 2003.
- [37] S. W. Chang, T. R. Lin, and S. L. Chuang, "Theory of plasmonic Fabry-Perot nanolasers," *Opt. Express*, vol. 18, pp. 15039–15053, 2010.
- [38] H. D. Sun *et al.*, "Stimulated emission induced by exciton-exciton scattering in ZnO/ZnMgO multiquantum wells up to room temperature," *Appl. Phys. Lett.*, vol. 77, 2000, Art. no. 4250.
- [39] D. M. Bagnall *et al.*, "High temperature excitonic stimulated emission from ZnO epitaxial layers," *Appl. Phys. Lett.*, vol. 73, 1998, Art. no. 1038.
- [40] T. Guillet *et al.*, "Laser emission with excitonic gain in a ZnO planar microcavity," *Appl. Phys. Lett.*, vol. 98, 2011, Art. no. 211105.
- [41] C. Klingshirn, R. Hauschild, J. Fallert, and H. Kalt, "Room-temperature stimulated emission of ZnO: Alternatives to excitonic lasing," *Phys. Rev. B*, vol. 75, Mar. 2007, Art. no. 115203.
- [42] J. C. Johnson, H. Q. Yan, P. D. Yang, and R. J. Saykally, "Optical cavity effects in ZnO nanowire lasers and waveguides," *J. Phys. Chem. B*, vol. 107, pp. 8816–8828, Aug. 2003.
- [43] R. Ambigapathy *et al.*, "Coulomb correlation and band gap renormalization at high carrier densities in Quantum wires," *Phys. Rev. Lett.*, vol. 78, pp. 3579–3582, May 1997.
- [44] K. Ding, J. O. Diaz, D. Bimberg, and C. Z. Ning, "Modulation bandwidth and energy efficiency of metallic cavity semiconductor nanolasers with inclusion of noise effects," *Laser Photon. Rev.*, vol. 9, pp. 488–497, Jul. 2015.

Yu-Hsun Chou received the B.S. degree in physics from National Cheng Kung University, Tainan, Taiwan, in 2010, and the Ph.D. degree from the Institute of Lighting and Energy Photonics, National Chiao Tung University, Hsinchu, Taiwan. His research interests include modeling, measurement and characterization of nanophotonic, and plasmonic devices.

Kuo-Bin Hong received the M.S. and Ph.D. degrees from the Institute of Applied Mechanics, National Taiwan University, Taipei, Taiwan, in 2003, and 2010, respectively. His current research interests include theoretical calculations of optical properties of quantum dot-based semiconductor nanostructures, modeling and simulation of photonic crystal surface emitting lasers, vertical cavity surface emitting lasers, plasmonic nanolasers, and other optoelectronic devices.

Yi-Cheng Chung received the B.S. and M. S. degrees in mechanical engineering from National Taiwan Ocean University, Keelung, Taiwan, in 2014 and 2015, respectively. He is currently working toward the Ph.D. degree at the Department of Mechanical and Mechatronic Engineering, National Taiwan Ocean University, Keelung. His current research interests include numerical simulation of plasmonics and semiconductor nanolasers.

Chun-Tse Chang received the B.S. degree in physics from Fu Jen Catholic University, New Taipei City, Taiwan, in 2015. He is currently working toward the M.S. degree at the Department of Photonics, National Chiao Tung University, Hsinchu, Taiwan. His current research interests include modeling, measurement and characterization of nanophotonic, and plasmonic devices.

Bo-Tsun Chou received the B.S. degree in electrical engineering from the National Taiwan Ocean University, Keelung, Taiwan, in 2008, the M.S. degree in electronic engineering from the National Chiao Tung University, Hsinchu, Taiwan, in 2010, and the Ph.D. degree from the Department of Electronic Engineering, National Chiao Tung University, Hsinchu. His current research interests include design, fabrication, simulation, and characterization of nanophotonic and plasmonic devices. He received the Outstanding Teaching Award 2013 at National Chiao Tung University.

Tzy-Rong Lin (M'12) received the Ph.D. degree in the applied mechanics from the National Taiwan University, Taipei, Taiwan, in 2006. He was the Postdoctoral Fellow in the Institute of Applied Mechanics, National Taiwan University, from 2006 to 2007, and in the Department of Electrical and Computer Engineering, University of Illinois at Urbana-Champaign, Urbana, IL, USA, from 2007 to 2009, respectively. In 2009, he joined National Taiwan Ocean University, Keelung, Taiwan, where he is currently an Associate Professor in the Department of Mechanical and Mechatronic Engineering, and an Adjunct Associate Professor in the Institute of Optoelectronic Sciences. He was a Visitor at the University of Illinois at Urbana-Champaign, in 2010. His current research interests include plasmonic semiconductor nanolasers, and mechanical and optoelectronic coupling in semiconductor nanostructures including strained semiconductor quantumwell and quantum-dot lasers, and optomechanical devices. He is a Member of the Optical Society of America and the American Society of Mechanical Engineers. He received the Yen Tjing Ling Award from Yen Tjing Ling Industrial Development Foundation, in 2007, the Excellent Teaching Award, in 2013, the Excellent Research Award, in 2014, from National Taiwan Ocean University, and the Merry Electro-Acoustic Award from Merry Electronics Co., Ltd., in 2014.

Sergei M. Arakelian received the Graduation (Hons.) degree from the Department of Physics, Yerevan State University (YSU), Yerevan, Armenia, in 1971. He was working on the MS-project at the Lomonosov Moscow State University (MSU), Moscow, Russia. Later he took graduate courses at this University. He received the Ph.D. degree in physics and mathematics (scientific interests – laser physics, statistical, and coherent/nonlinear optics) from MSU, in 1975, and also the Senior Doctor in physics and mathematics (nonlinear spectroscopy and laser physics) at the MSU in 1988. Since 1988, he has been a Professor of the Department of Optics, and since 1990, has been the Chairman of the Department of Molecular Physics and Laser Biophysics, YSU. Since 1992, he has been a Professor of the Department of Physics and Applied Mathematics, since 1994 he has been the Chairman of the above mentioned department at Vladimir State University, Vladimir, Russia. In 1995, he was elected as an active member of the Russian Academy of Engineering Sciences. He was a Postdoctoral (study for nonlinear optics of liquid crystals) in the Department of Physics, University of California, Berkeley, CA, USA, during 1980–1981. He also worked there as a Visiting Professor in 1985. In 1981, he became a member of the American Optical Society. He is considered to be a noted expert in the fields of laser, coherent and non-linear optics, optical instabilities, as well as in the field of quantum information systems and technologies. He is the author of more than 200 profound scientific papers published in refereed scientific journals, patents, and monographs in the field of highly precise measurement with laser beams and in developing of new physical principles to create the quantum optical information systems with ultimate characteristics at the level of quantum limitations.

Alexander P. Alodjants received the Master's degree (Hons.) in theoretical physics from Department of Physics, Yerevan State University, Yerevan, Armenia, in 1990. He received the Ph.D. degree in laser physics from M.V. Lomonosov Moscow State University (MSU), Moscow, Russia, in 1993. He received the Doctor of Science (Doctor in Physics and Mathematics) degree in laser physics from the Laser Physics Institute, Russian Academy of Sciences, Novosibirsk, Russia, in 2010. During 1993–1995, he was appointed as a Post-doctoral in the International Laser Center, MSU, in the field of quantum optics and quantum information theory. During 1995–2016, he was the Professor in the Department of Physics and Applied Mathematics, Vladimir State University. Since 2017, he has been a Professor in Department of Quantum Optics and Laser Physics, ITMO University, Saint Petersburg, Russia. Since 1997, he has been appointed as a Guest Researcher at Optics Division, Erlangen University, Erlangen, Germany, and at the Department of Theoretical Physics, Innsbruck University (during 1999–2000), in Bonn University, Germany (2007), in Russian Quantum Center, Skolkovo (during 2013–2015). He is the author of more than 70 peer-reviewed research papers published in high level international journals. His research interests include the field of quantum optics, photonics, condensed matter physics are connected with the theoretical research of the fundamental quantum and classical phenomena taking place under the interaction of photons with atoms, low-dimensional spatio-periodical systems, and semiconductor micro- and nanostructures. His scientific activity was highly appreciated by Soros and Dynasty Foundations, European Academy.

Tien-Chang Lu (M'07–SM'12) received the B.S. degree in electrical engineering from the National Taiwan University, Taipei, Taiwan, in 1995, the M.S. degree in electrical engineering from the University of Southern California, Los Angeles, CA, USA, in 1998, and the Ph.D. in electrical engineering and computer science from National Chiao Tung University, Hsinchu, Taiwan, in 2004. He was with the Union Optronics Corporation as a Manager of Epitaxy Department in 2004. Since August 2005, he has been with National Chiao Tung University as a full-time Professor in the Department of Photonics. In 2007, he went to Ginzton Lab, Department of Applied Physics, Stanford University as a Visiting Scholar. He served as the Director of the Institute of Lighting and Energy Photonics, National Chiao Tung University from 2009 to 2011. Since 2017, he has been serving as the Director of Tin Ka Ping Opto-Electronics Research Center. His research interests include the design, epitaxial growth, process, and characterization of optoelectronic devices. He has been engaged in the low-pressure MOCVD epitaxial technique associated with various material systems as well as the corresponding process skills. He is also interested in tailoring the light-matter interaction in micro- or even nanoscale architectures, such as the microcavity, photonic crystal and plasmonic structures. Prof. Lu has authored and coauthored more than 200 international journal papers. He received the Exploration Research Award of Pan Wen Yuan Foundation 2007, the Excellent Young Electronic Engineer Award 2008, the Young Optical Engineering Award 2010, the International Micro-Optics Conference Contribution Award 2011, Dr. Ta-Yu Wu's Memorial Award 2012, and Y. Z. Hsu Scientific Paper Award 2016. He is a member of OSA and SPIE. He also served as Deputy Editors of the IEEE JOURNAL OF LIGHTWAVE TECHNOLOGY, Associate Editors of the IEEE JOURNAL OF QUANTUM ELECTRONICS and *Chinese Optics Letters*.